Title: Disrupted neuro-glial metabolic coupling after peripheral surgery

Abbreviate title: Peripheral surgery and brain function

Author names and affiliation: Femenía, Teresa[1]; Giménez-Cassina, Alfredo[2,3]; Codeluppi, Simone[2,4]; Fernández-Zafra, Teresa[4]; Katsu-Jiménez, Yurika[2]; Terrando, Niccolò[5,6]; Eriksson, Lars I[1]; Gómez-Galán, Marta[1]

[1]Department of Physiology and Pharmacology, Section for Anesthesiology and Intensive Care Medicine, Karolinska Institutet. Stockholm, 171 77, Sweden.

[2]Department of Medical Biochemistry and Biophysics. Karolinska Institutet. Stockholm, 171 77, Sweden.

[3]Department of Biología Molecular, Universidad Autónoma de Madrid, Centro de Biología Molecular "Severo Ochoa" (CSIC-UAM), Spain

[4]Department of Physiology and Pharmacology, Karolinska Intitutet, Stockholm, Sweden

[5]Department of Anesthesiology, Basic Science Division, Duke University Medical Center, Durham, NC 27710, USA.

[6]Center for Translational Pain Medicine, Duke University Medical Center, Durham, NC 27710, USA.

Corresponding author: Gómez-Galán Marta; Department of Physiology and Pharamacology, Section for Anesthesiology and Intensive Care Medicine, Karolinska Institutet. Nanna Svart 2, Stockholm, 171 77, Sweden; E-mail: marta.gomez@ki.se

Number of pages: 41

Number of Figures: 7

Number of words:

Abstract: 244

Introduction: 524

Discussion: 1536

Conflict of interest: The authors declare no conflict of interest

Acknowledgment: The authors thank Anette Ebberyd for excellent technical support, Souren Mkrtchian for critically reading the manuscript, Lilly Schwieler for assistance with the multiplex cytokine analysis, Enric Domènech-Estévez for the mcts antibodies and Mia Lindskog for kindly allow us to use her patch-clamp set up system. AGC was supported by a "Ramón y Cajal" fellowship (RYC-2014-15792) from Spanish "Ministerio de Economía y Competitividad". This work was funded by the Swedish Research Council and the confocal microscope used in the study by Knut and Alice Wallenberg Foundation [Grant KAW2008.0149]. NT is supported by NIH/NIA R01AG057525.

Abstract

Immune-related events in the periphery can remotely affect brain function, contributing to neurodegenerative processes and cognitive decline. In mice, peripheral surgery induces a systemic inflammatory response associated with changes in hippocampal synaptic plasticity and transient cognitive decline, however the underlying mechanisms remain unknown. Here we investigated the effect of peripheral surgery on neuronal-glial function within hippocampal neuronal circuits of relevance to cognitive processing in male mice at 6, 24, and 72h post-surgery. At 6h we detect the pro-inflammatory cytokine IL-6 in the hippocampus, followed up by alterations in the mRNA and protein expression of astrocytic and neuronal proteins necessary for optimal energy supply to the brain and for the reuptake and recycling of glutamate in the synapse. Similarly, at 24h post-surgery the mRNA expression of structural proteins (GFAP and AQP4) was compromised. At this time point, functional analysis in astrocytes revealed a decrease in resting calcium signaling. Examination of neuronal activity by whole-cell patch clamp shows elevated levels of glutamatergic transmission and changes in AMPA receptor subunit composition at 72h post-surgery. Finally, lactate, an essential energy substrate produced by astrocytes and critical for memory formation, decreases at 6- and 72h after surgery. Based on temporal parallels with our previous studies, we propose that the previously reported cognitive decline observed at 72h post-surgery in mice might be the consequence of temporal hippocampal metabolic, structural and functional changes in astrocytes that lead to a disruption of the neuro-glial metabolic coupling and consequently to a neuronal dysfunction.

Significance Statement

A growing body of evidence suggests that surgical trauma launches a systemic inflammatory response that reaches the brain and associates with immune activation and cognitive decline. Understanding the mechanisms by which immune-related events in the periphery can influence brain processes is essential for the development of therapies to prevent or treat postoperative cognitive dysfunction and other forms of cognitive decline related to immune-to-brain communication, such as Alzheimer's and Parkinson's diseases. Here we describe the temporal orchestration of a series of metabolic, structural and functional changes after aseptic trauma in mice related to astrocytes and later in neurons that emphasize the role of astrocytes as key intermediaries between peripheral immune events, neuronal processing, and potentially cognition.

Introduction

Despite the classical view of the central nervous system (CNS) as an immune privilege organ, growing evidence points to an active crosstalk between the peripheral immune system and the CNS, which suggests that immune-related events in the periphery can remotely affect brain function, contributing to neurodegenerative processes and cognitive decline (Perry et al., 2003).

Activation of the peripheral innate immune system after trauma (e.g. surgery) leads to the increase of pro-inflammatory cytokines in both the systemic circulation and the CNS. Importantly, this increase in cytokines has been associated with prolonged impairment in learning and memory (Buvanendran et al., 2006; Beloosesky et al., 2007; Kline et al., 2016). Recently, the first PET study of the human brain immune activity after surgery using PBR28, a novel translocator protein (TSPO) ligand, revealed a profound postoperative dysregulation of brain glial activity even at 3 to 4 months after surgery associated with poor cognitive outcome (Forsberg et al., 2017). In surgical rodent models, such periphery-to-brain inflammatory pathway seems critically dependent on NF-kB and pro-inflammatory cytokine signaling (e.g., tumor necrosis factor-a [TNF-a]), associated with a transient disruption of blood–brain barrier (BBB) integrity, migration of peripheral macrophages into the hippocampus, and subsequent cognitive impairment (Terrando et al., 2010; Terrando et al., 2011; Degos et al., 2013; Yang et al., 2017). However, the consequence of this periphery-to-brain signaling on hippocampal function remains largely unknown. We recently demonstrated that surgery-induced cognitive decline in mice was associated with hippocampal astrocytic morphology alteration and synaptic plasticity impairment. Notably, the astrocytic change preceded the neuronal impairment (Terrando et al., 2013), suggesting that primary changes in astrocyte function have the potential to modulate large-scale

93 neuronal functional systems. With its typical location having one part of the cell attached to
94 the vascular wall and the other part in close proximity to the synapse, astrocytes emerge as
95 pivotal mediators between the periphery and neuronal functions. However, the effects of
96 systemic immune activation and inflammation on astrocyte functions are not well defined.
97 In the last decade, a large body of evidence suggests that an array of systemic challenges
98 (including surgery) can promote a systemic inflammatory response that may contribute to
99 the exacerbation of acute symptoms of chronic neurodegenerative disease, such as
100 Alzheimer's disease (AD) and Parkinson's disease (PD), thus accelerating disease progression
101 (Perry et al., 2007; Collins et al., 2012). Indeed, a series of disease-generating mechanisms
102 observed after peripheral trauma have also been described on these and other brain
103 disorders associated with cognitive dysfunction, such as BBB disruption and infiltration of
104 activated macrophages (Lebson et al., 2010; Birch et al., 2014; Perry and Holmes, 2014).
105 To further understand the temporal pattern of immune activation and simultaneous changes
106 in synaptic transmission within hippocampal neuronal circuits of relevance for cognitive
107 processing, we investigated the effect of surgery on neuronal-glial function combining
108 calcium (Ca^{2+}) imaging in astrocytes and whole-cell patch clamp in CA1 pyramidal cells with
109 structural and metabolic analysis in mice. Our findings uncover a role for astrocytes as
110 mediators between systemic immune and inflammatory events and synaptic neuronal
111 functions including a dysregulation of brain energy metabolism, which may be in turn related
112 to the surgical phenotype, including cognitive impairment post-surgery.
113

Material and Methods

Animals

All experiments were approved by the Local Ethics Committee for Animal Research at Karolinska Institutet (Stockholm, Sweden) and comply with the Society for Neuroscience policy on the use of animals in research. Male, 12-14 weeks old C57BL6 (Charles River, Germany) and $CX3CR1^{GFP/+}CCR2^{RFP/+}$ mice (generated as previously described (Saederup et al., 2010) and kindly donated by Akassoglou K, J. David Gladstone Institutes, San Francisco, California, USA) were used. Mice were housed 6/cage under temperature- and humidity-controlled conditions with 12-h light-dark cycle and fed standard rodent chow and water *ad libitum*. All animals were weighted just before surgery (or saline injection in the case of the naïve animals) and before brain collection.

Surgery

The open stabilized tibia fracture model was performed as previously described (Terrando et al., 2013). Briefly, under isoflurane anesthesia (2.1% inspired concentration in 0.30 FiO_2) and analgesia (buprenorphine, 0.1 mg/kg s.c.) a longitudinal incision was made on the left hind paw and the muscles disassociated. A 0.38-mm stainless steel pin was then inserted in the intramedullary canal and the osteotomy was performed. The wound was irrigated, sutured with 6-0 Prolene, and the mice were allowed to recover in a warm box before returning to the home cage. The procedure lasted 21 ± 0.5 min. Temperature was monitored and maintained at 37°C with the aid of a warming pad and temperature controlled lights (Harvard Apparatus, Holliston, MA, USA). Animals sacrificed at 24-72h post-surgery received a daily dose of analgesia (buprenorphine, 0.1 mg/kg s.c.) during the length of the study. Control mice received an equal volume of saline (s.c.).

Acute brain slices

Mice were terminated at 6-24-72 hours after tibia fracture completion by cervical dislocation. The brain was quickly harvested following decapitation and the whole hippocampus removed into ice-cold oxygenated (95% O_2 and 5% CO_2) artificial cerebrospinal fluid solution (aCSF) containing (in mM): 130 NaCl, 3.5 KCl, 1.25 NaH_2PO_4, 24 $NaHCO_3$, 2 $CaCl_2$, 1.5 $MgCl_2$, and 10 glucose, pH 7.4 (330 mOsmol). Horizontal hippocampal slices (400 μm) were prepared with a vibratome (VT1200S, Leica), and the slices were incubated for 20 min in an interface chamber containing oxygenated aCSF warmed at 34°C and then left for approximately 40 min at room temperature.

Ca^{2+} imaging

Mouse brain slices were prepared as described previously. After recovering, slices containing the hippocampus were transferred to a customized loading chamber: a millicell culture insert for organotypical cultures (Millicell; Merk-Millipore, Germany) fitted in a 35mm petri-dish and placed into a 100 mm petri-dish with bubbling tubing glued around it and a lid with a gas entrance to allow continuous oxygenation (95% O2 and 5% CO2). Both, the 35 mm and 100 mm petri-dishes were filled with regular aCSF (1150 μl and 5 ml, approximately).

Loading and mounting. To identify hippocampal astrocytes, slices were first loaded with Sulforhodamine 101 (S101) for 15 min, washed and loaded with the Ca^{2+} indicator dye Oregon Green 488 BAPTA-1 AM (OGB-1, 50 μg) previously dissolved in a solution containing: 9 μl 0.5% Cremophor EL (in DMSO) + 1μl Pluronic F127 (in DMSO) + 10μl regular aCSF (20 μM OGB-1; 0.002 μM Cremophor EL; 0.01% Pluronic F127; 0.5% DMSO). A 5μl drop of the OGB-1 dye solution was placed on top of each individual slice and incubated for 45-60 min at 37 °C. After that period, the aCSF was replaced for fresh aCSF and the slices recovered for 30 min at room temperature. For Ca^{2+} imaging, slices were

mounted upside-down in bottom glass culture dishes (MatTek Corporation, USA) pre-coated with PEI (1ml for 1h at room temperature and rinsed 3-5 times with distilled water and aCSF). To avoid possible detachment during imaging, the borders of the slices were carefully dried with the help of a filter paper and the slice gently covered with 1ml of aCSF. Once mounted, the slices were kept in the oxygenated chamber before being transferred individually to the recording chamber (Warner Instruments, USA).

Imaging. Slices were continuously perfused with aCSF at room temperature and astrocytes were identified in the CA1 area with a 25X objective in an upright laser-scanning confocal microscopy (LSM 710 from Carl Zeiss, Germany). S101 was excited at 568 nm and collected through a 630 long-pass filter while OGB-1 was excited at 488 nm and collected through a 522±16 nm band-pass filter.

Spontaneous astrocytic Ca^{2+} transients were recorded from live hippocampal astrocytes loaded with both OGB-1 and S101 in time-series images of 300-600 frames collected at 1 s intervals. At the end of the experiments, ATP (100nM) was applied to monitor typical calcium responses of astrocytes. The slices that did not respond to ATP were excluded for the analysis.

The acquired image stacks were registered using the turboreg plugin (Thevenaz et al., 1998) of Fiji (RRID:SCR_002285) (Schindelin et al., 2012). The cells were then identified as connected components of the binary images after semi-automated thresholding and size filtering of the SR101 immunofluorescence. The signal intensity of OGB-1AM in each cell was quantified and exported from Fiji (RRID:SCR_002285) to be further processed using a custom python script. The fluorescence signal was converted in dF/F0 where F0 was the mean fluorescence signal of the trace, and all the peaks in the trace were labeled. A response was defined as a peak with dF/F0 above 10 % of F0.

Electrophysiology

For whole-cell voltage clamp recordings of CA1 pyramidal cells, after slice recovery, a single slice was transferred to a submersion recording chamber, where it was continuously perfused (1.8–2 ml/min) with regular aCSF warmed to 31–32°C. Patch electrodes (4–6 MΩ) were filled with a solution containing (in mM): 110 (for excitatory postsynaptic currents (EPSCs)) or 20 (for inhibitory PSCs (IPSCs)) K-gluconate, 10 (for EPSCs) or 100 (for IPSCs) KCl, 4 Mg_2-ATP, 10 phosphocreatine, 0.3 Na_2-GTP and 10 HEPES, pH 7.3 with KOH (270–290 mOsm). Cells were voltage clamped at -65mV, and either spontaneous EPSCs or IPSCs were recorded using a Multiclamp 700B amplifier (Molecular Devices, Sunnyvale, CA, USA). The data were acquired using pCLAMP 10 (Molecular Devices, Sunnyvale, CA, USA). Recordings with a membrane potential (Vm) more positive than -55mV and/or access resistances (Rs)>30 MΩ were excluded, and only cells with stable Rs and Vm (i.e., a change of <10%) were included in the analysis. All PSCs were analyzed using Mini Analysis software (Synaptosoft, Decatur, GA, USA). Detection criteria included EPSCs and IPSCs with an amplitude >7.5 pA and a 20–80% decay-rise time >0. Data represent the average of 3 min of recording. The numerical values are expressed as the mean± SEM and n indicates the number of neurons tested.

Brain collection

Animals were cardially perfused with cold PBS (20ml) and the hippocampus dissected and wet weighted in lock-safe tubes and stored at -80°C until further analysis.

Preparation of brain tissue for cytokine analysis

Hippocampal samples from cold PBS cardially perfused animals were homogenized in ice-cold lysis buffer (100mg/ml) (in mM): 150 NaCl, 20 Tris pH 7.5, 1 EDTA; 1 EGTA; 1% triton X-100; protease inhibitor (Roche, Sigma-Aldrich); Phosphatase Inhibitor Cocktail 3

(Sigma-Aldrich) Phosphatase Inhibitor 2 (Sigma-Aldrich); 200ul NaF (from 0.5M stock), with glass beads for 3-5 minutes with speed 8 at 4°C using a Bullet-Blender (Next Advance, Averill Park, NY). Homogenates were then centrifuged 14 000 rpm for 10 min at 4°C. Cytokines were directly analyzed the same day following the multiplex cytokine assay protocol (see below).

Multiplex cytokine assay

Brain pro- and anti-inflammatory cytokine levels were determined with Mouse Pro-inflammatory 10 Plex Ultrasensitive Plate (IFN-gamma, IL-1β, IL-2, IL-4, IL-5, IL-6, IL-10, IL-12 p70, KC/GRO (CXCL1), and TNF-α) from Meso Scale Discovery (Rockville, USA) at 6-72h after tibia fracture completion according to manufacturer's instructions.

Western Blot (WB)

Hippocampal samples were homogenized in 1% sodium dodecyl sulphate (SDS) buffer containing protease and phosphate inhibitors (Sigma-Aldrich). Protein concentration was determined using the BCA Protein Assay Kit (Thermo Scientific) and equal amounts of protein (20–30μg) were resolved by SDS-PAGE and transferred onto a PVDF membrane (Invitrogen). Detection was done by enhanced chemiluminescence with Amersham ECL western blotting detection reagents (GE Healthcare). Chemiluminescence was determined with a ChemiDoc MO analyzer (Bio-Rad). Band intensities were quantified by densitometry using ImageJ software (NIH, Bethesda, MD, USA). Ponceau S staining of the membrane was used as a loading control (Romero-Calvo et al., 2010). Primary antibodies were rabbit monoclonal anti-glutamate Receptor 1 (AMPA subtype) (1:1000, Abcam Cat# ab109450 RRID:AB_10860361); rabbit polyclonal anti-glutamate Receptor 2 (1:1000, Abcam Cat# ab20673 RRID:AB_2232655); rabbit polyclonal anti-EAAT1 (GLAST) (1:5000; Abcam Cat# ab416 RRID:AB_304334); rabbit polyclonal anti-EAAT2 (GLT-1) (1:5000; Abcam

Cat# ab41621 RRID:AB_941782); rabbit polyclonal anti-Glutaminase (1:1000; Abcam Cat# ab93434 RRID:AB_10561964); rabbit monoclonal anti-Glutamine Synthetase (1:1000; Abcam: AB176562); rabbit monoclonal anti-Glucose Transporter GLUT3 (1:5000; Abcam: AB191071), rabbit monoclonal anti-Glucose Transporter GLUT1 (1:50.000; Abcam Cat# ab115730 RRID:AB_10903230); rabbit polyclonal anti-MCT1 (1:500; Santa Cruz Biotechnology Cat# sc-50325 RRID:AB_2083632); goat polyclonal anti-MCT2 (1:500; Santa Cruz Biotechnology Cat# sc-14926 RRID:AB_2187245); rabbit polyclonal anti-MCT4 (1:500; Santa Cruz Biotechnology Cat# sc-50329 RRID:AB_2189333).

Quantitative Real Time PCR analysis (qRT-PCR)

The hippocampus was rapidly dissected on ice and frozen on dry ice and stored at -80C until used. Total RNA was isolated using Isol-RNA lysis reagent (5 PRIME, Inc. Galthersburg, USA) according to the manufacturer's instructions, and quantified by spectrophotometry using a NanoDrop ND-1000 Spectrophotometer (NanoDrop Technologies, Wilmington, DE, USA). cDNA synthesis was performed first completing a DNase digestion step for removal of genomic DNA (Invitrogen, Stockholm, Sweden) (1U per 1ug of RNA), thereafter first-strand cDNA was carried out with equal amounts of total RNA (1 μg/ 20 μl reaction) using the iScript cDNA synthesis kit (BIO-RAD, Sundbyberg, Sweden) according to the manufacturer's instructions and diluted with nuclease free water up to 100 μl after reaction and stored at -20C until used. A total volume of 2 μl (housekeeping) 3 μl (rest of the genes) or 6 μl (cytokines) was used for gene expression analyses, together with 10 μl SYBR® Select Master Mix (Applied Biosystems), 0.5 μM of each primer and nuclease free water up to a reaction volume of 20 μl. Taq-man pre-designed probes and TaqMan® Fast Advanced Master Mix were used for glucose transporters (Glut1 and Glut3) as well for the housekeeping TATA-box binding protein (Tbp) (Thermofisher Scientific) and prepared

following the manufacture instructions. Real-time PCR was carried out using the iCycler Real-Time PCR Detection System (Applied Biosystems). The sequences of the used primers are listed bellow (F, forward, R, reverse):

Mct1 F_aatgctgccctgtcctccta, Mct1 R_cccagtacgtgtatttgtagtctccat;

Mct2 F_cagcaacagcgtgatagagct, Mct2 R_tggttgcaggttgaatgctaa;

Mct4 F_cagctttgccatgttcttca, Mct4 R_agccatgagcacctcaaact;

Gfap F_ggggcaaaagcaccaaagaag, Gfap gggacaacttgtattgtgagcc;

Aqp4 F_gagtcaccacggttcatgga, Aqp4 R_cgtttggaatcacagctggc;

Gs F_tgaacaaaggcatcaagcaaatg, Gs R_cagtccagggtacgggtctt;

Gls F_gctgtgctctattgaagtgaca, Gls R_ttgggcagaaaccaccattag;

Actin F_gatgtatgaaggctttggtc, Actin R_tgtgcacttttattggtctc

Slc2a1 (Glut1) Taqman probe Mm 00441480_m1; Slc2a3 (Glut3) Taqman probe Mm 00441480_m1.; Tbp Taqman probe Mm00446973_m1.

The housekeeping gene β-actin or Tbp were used as endogenous control for normalization. The data analysis was based on the $2^{-\Delta\Delta Ct}$ method. The normalized ΔCt for each gene was calculated by subtracting the Ct of the reference gene actin from the Ct of each target gene. Then, the double delta Ct (ΔΔCt) for each gene was calculated by deducting the average ΔCt of the target gene of the control group from the ΔCt of each target gene in the surgery group. The fold changes of the surgery group compared with the control group were calculated as $2^{-\Delta\Delta Ct}$.

Immunohistochemistry (IHC)

Mice were sacrificed and perfused with saline followed by 4% paraformaldehyde in 100 mM phosphate buffer. Their brains were removed, post-fixed in the same fixative overnight (4°C), and then immersed in 30% sucrose for 48 hours. Brains were then embedded in

optimal cutting temperature compound, immediately frozen on dry ice, and stored (–80ºC). Coronal sections (25-µM thick) were cut on a cryostat, mounted on glass slides using Vectashield antifade mounting media (Vector Labs; catalog H-1200), blocked for 1 hour with 5% BSA (Sigma-Aldrich) in PBS containing 0.1% Triton X-100 (Fisher Scientific), and incubated over night with an anti-GFAP antibody (1:500 rabbit polyclonal; Dako). Immunofluorescence was performed with Alexa Fluor Cy3–labeled anti–rabbit DAPI Vectashield solution (Vector Labs) to identify cell nuclei. Images were acquired by confocal laser-scanning microscopy (LSM 710 from Carl Zeiss, Germany).

Image Analyses

Images of the CA1 region of the hippocampus (left and right) stained for DAPI and GFAP were acquired with an inverted laser scanning confocal microscope (LSM 800) equipped with a 20X/0.8 air objective and ZEN2 (blue edition) software (Carl Zeiss, Germany). All images were taken using the same intensity settings and the person acquiring the images was blinded to the experimental conditions. Images were acquired using the z-stack function, sampling 5 different depths 1um apart from the focal center of the tissue. Z-stacks images were post-processed and analyzed with Image J software (RRID:SCR_003070).

Lactate

Approximately 10-25 mg of tissue was homogenized in 1 ml of a dry-ice chilled solution containing 80% methanol in H_2O. The homogenates were then incubated at -20ºC over night, and they were then centrifuged at 12,000 rpm x 15 min to remove the insoluble fraction. The supernatants, containing soluble metabolites, were then lyophilized and subsequently re-suspended in 50 µl of sterile H_2O. The amount of lactate present in the supernatants was determined using the LACT reagent from Beckman-Coulter (Brea, CA,

USA), according to the manufacturer´s guidelines. The results were then normalized by the starting amount of tissue used to prepare the homogenate.

Experimental design and Statistical Analysis

An aseptic orthopedic surgery was performed on male C57BL6 and CX3CR1$^{GFP/+}$CCR2$^{RFP/+}$ mice under anesthesia and analgesia conditions. On average the total anesthesia time (including the induction time) was 22.2 ±1. min and animals recovered from it in about 2-5 min. Experimental groups were randomly divided in three groups and sacrificed by cervical dislocation at three different time points: 6-24 and 72h post-surgery. The 24 and 72h group received a daily dose of analgesia to avoid the possible effect of pain on the brain. To avoid experimental variation over time, control animals from the same batch of animals were assigned to each of the groups and received a daily injection of saline (s.c). However, since no statistical difference was found in any of the performed experiments, all controls were pooled as a single group. The number of animals assigned per group was determined from previous experiences in the field and included into the results section for each experiment.

Statistical analyses were performed using Prism Version 6 software (GraphPad; RRID:SCR_002798). D'agostino & Pearson omnibus normality test was used to test normality of values distribution. Significance of difference was analyzed using unpaired two-tailed Student's t test for single comparisons or ANOVA one-way test analysis followed by Fisher's multiple comparisons test. In cases of variances that were not assumed to be equal, a Welch correction was performed. Data are presented as means ± SEM. $P<0.05$ was considered significant.

Results

1. Brain cytokine levels after peripheral surgery

It has been previously reported that tibia fracture increases both the systemic and hippocampal expression levels of the pro-inflammatory cytokines, IL-1β and IL-6 at 6h post-surgery (Cibelli et al., 2010; Terrando et al., 2010; Fidalgo et al., 2011; Lu et al., 2015). To further explore the presence of these and other inflammatory cytokines in the brain after tibia fracture, we determined the protein levels of several hippocampal pro- and anti-inflammatory cytokine by multiplex analysis (Figure 1). From all the cytokines tested (IFN-gamma, IL-1β, IL-2, IL-4, IL-5, IL-6, IL-10, IL-12 p70, KC/GRO/CXCL1, and TNF-α) we found an increase in IL-6 at 6h after tibia fracture, returning to control values at 72h post-surgery (Figure 1B; ***p=0.0002 C vs. S6H; #p=0.01 S6H vs. S72H; one-way ANOVA, Fisher's multiple comparisons test; n=5-10 animals/group). Notably, in opposition to those studies that found increased IL-1β at 6 post-surgery (Cibelli et al., 2010; Fidalgo et al., 2011) we did find reduced IL-1β at 6 post-surgery reversed by 72h (Figure 1B; *p=0.03 C vs. S6H; ##p=0.0095 S6H vs. S72H; one-way ANOVA, Fisher's multiple comparisons test; n=4-10 animals/group). Similarly, Rosczyk at al., (2008), comparing adults against aged animals, observed that while aged mice showed an increase IL-1β mRNA in the hippocampus after surgical trauma, adult mice showed control values of IL-1β mRNA implying that aging might be a critical factor regarding to the presence of IL-1β after peripheral surgery.

2. Peripheral surgery regulates expression of astrocytic markers

Cytokines, including IL-6, can cross the BBB via saturable transport (Banks et al., 1994; Gutierrez et al., 1994; Banks et al., 1995; Banks, 2005) to act directly on astrocytes, microglia and neurons. Previously, we have shown that 24h after tibia fracture, hippocampal $GFAP^+$

astrocytes from the stratum radiatum (SR) are morphologically altered, with astrocytes presenting shorter processes and reduced GFAP coverage. These changes were completely reversed at 72h post-surgery (Terrando et al., 2013). Hence, we sought to explore the effect of tibia fracture on the expression of two main astrocytic markers, GFAP and AQP4. Time-course studies were performed in hippocampal homogenates from control and surgery-treated animals between 6-, 24- and 72h following tibia fracture (Figure 2). Compared to naïve animals, the mRNA expression of both gfap and aqp4 was decreased at 24- and 72h post-surgery (Figure 2; gfap: *p=0.02 at 24H and *p=0.04 at 72H; n=5-16 animals; aqp4: *p=0.04 at 24H and *p=0.01 at 72H; n=4-12; one-way ANOVA, Fisher's multiple comparisons test).

3. Resting Ca^{2+} signaling is decreased in the hippocampal astrocytic network after surgery

In order to evaluate the functional consequences of peripheral surgery on astrocytes we monitored spontaneous intracellular Ca^{2+} transients in a population of cells loaded with both, the calcium indicator OGB-1 and the astrocytic marker SR101 at 24h after tibia fracture (Figure 3A). This technique allowed us to selectively identify astrocytes among other brain cells (neurons and microglia) since in the hippocampus SR101 is taken up mainly by $GFAP^+$ astrocytes (Kafitz et al., 2008). Nevertheless, in recent years some authors suggest that oligodendrocyte labeling may occur through transfer from astrocytes via gap-junction coupling between these two cell populations (Hill and Grutzendler, 2014).

We analyzed the spontaneous Ca^{2+} activity in 19 and 14 hippocampal slices, from 5 control and 4 surgery-treated animals. We first observed that the number of labeled astrocytes ($SR101^+$ cells) was significantly reduced in slices from 24h surgery-treated animals compared to hippocampal slices from control animals (Figure 3D; 35 ± 2.6 vs. 49 ± 3; **p=0.002;

unpaired t-test; n=19-14 slices). This difference in number might be due to the reduced astrocytic GFAP coverage previously described in these animals (Terrando et al., 2013), which could make the detection of staining more difficult. However, to rule out this possibility, we analyzed the number of $GFAP^+$ cells by immunohistochemistry and found no differences compared to control (Figure 3E; p=0.29; t-test; n=8-10 animals, unpaired t-test). Notably, we found a profound decrease in GFAP immunoreactivity (Figure 3F-G; p=0.0019; t-test; n=6-9 animals, unpaired t-test), which correlate with the decrease in gfap expression already described (Figure 2A).

Next, we analyzed the percentage of active astrocytes per slice. Although the mean of the percentage of active cells did not reach significance (Figure 3H; 5.3 ± 0.8 % vs. 9.9 ± 2.6 %; p=0.08, unpaired t-test with Welch's correction; n=19-14 slices (7 animals/group)), the comparison of the variance was highly significant (###p=0.0001, F test to compare variances; F: 10.36; DFn: 18; Dfd: 13) indicating different subpopulation of astrocytes among groups. Then, we analyzed the frequency of the Ca^{2+} events detected during a 5-minute recording sequence, and found that the Ca^{2+} event frequency was higher in the control group (Figure 3I; 1.5 ± 0.1 vs. 1.1 ± 0.07 events per 5 min; *p=0.01; unpaired t-test with Welch´s correction; n=19-14 slices (4-5 animals/group)). We also recorded the Ca^{2+} response to ATP (100mM) during 5 min of bath application (Figure 3J). While the percentage of ATP responders was similar (not shown; 26.3 ± 6.1 % vs. 22.4 ± 4.1 %, C vs. S24H; n=10-15 slices; p=0.64, unpaired t-test) the frequency was significantly higher in the control group (Figure 3J; 2.1 ± 0.1 vs. 1.7 ± 0.1 events per 5min; *p=0.05; unpaired t-test with Welch´s correction; n=10-15 slices (7 animals/group)). Moreover, while astrocytes from hippocampal slices of naïve animals showed a heterogeneous functional profile with astrocytes able to fire 1 to 9 spikes/5min, Ca^{2+} signals from hippocampal slices of surgery-

treated animals did always show a single population of astrocytes firing 1 to 2 single Ca^{2+} spikes/5 min. Taken together these data suggest that peripheral surgery primarily changes the activity pattern among the most active subpopulation of hippocampal astrocytes.

4. Deficiency of glucose and lactate transporters is accompanied with changes in hippocampal lactate levels after peripheral surgery

A classical role attributed to astrocytes is to ensure an adequate metabolic supply to neurons. Astrocytes take up blood glucose through glucose transporters expressed in their end-feet and metabolize it to lactate, which is then delivered to neurons via lactate transporters to be used as an energy substrate in addition to glucose during high energy demands (Allaman et al., 2011) (see Figure 4A). Alterations in the regulation of this metabolic supply to neurons have been shown to have detrimental consequences in higher brain functions, such as cognition (Suzuki et al., 2011).

First, we analyzed the time course for the hippocampal lactate levels between 6-, 24- and 72h following tibia fracture. Compared to controls, lactate concentration was decreased at 6- and 72h after trauma, with normal levels at 24h (Figure 4B; *p=0.01 C vs. S6H; *p=0.047 C vs. S72H; p=0.7 C vs. S24H; n=5 animals/group; one-way ANOVA, Fisher's multiple comparisons test).

Second, we evaluated the expression pattern of the two main glucose transporters in the brain: GLUT-1 (expressed in the astrocytic end-feet) and GLUT-3 (expressed in neurons). Both, glut-1 and glut-3 gene expression was down-regulated at 6h after trauma (Figure 4C (top); glut-1: **p=0.0031, S6H vs. C; n=5-15; glut-3: ***p<0.0002 S6H vs. C; n= 5-15 animals, respectively; one-way ANOVA, Fisher's multiple comparisons test). Protein levels were decreased at 72h after surgery for GLUT-1 (Figure 4B (bottom)-C; *p=0.019, S72H vs. C; n=5 animals/group; one-way ANOVA, Fisher's multiple comparisons test) and decreased

422 at 24h and 72h for GLUT-3 (Figure 4C (bottom); **p=0.001, S24H vs. C; n=5/group;
423 **p=0.002, S72H vs. C; n=5-5 animals; one-way ANOVA, Fisher's multiple comparisons
424 test).
425 Finally, we analyzed the main brain lactate transporters, monocarboxylate transporters
426 (MCTs) 1, 2 and 4, being MCT1 and MCT4 expressed in astrocytes and MCT-2 in neurons.
427 Mct1 was significantly decreased at 6h, normal at 24h and decrease at 72h (Figure 4D (top);
428 *p=0.05 S6H vs. C; n=6-15 animals; *p=0.032, S72Hvs. C; n=5-15 animals; one-way
429 ANOVA, Fisher's multiple comparisons test); mct2 was significantly decreased at 72h
430 (Figure 4D (top); *p=0.042, S72H vs. C; n=5-15 animals; one-way ANOVA, Fisher's
431 multiple comparisons test), and mct4 dramatically increased at 24h (Figure 4D;
432 ****p<0.0001, S24H vs. C; n=5-14 animals; one-way ANOVA, Fisher's multiple
433 comparisons test). Western blot analysis of hippocampal homogenates did not revealed any
434 alteration in any of the brain lactate transporters tested (Figure 4D (bottom) and E).
435 **5. Peripheral surgery affects hippocampal proteins involved in glutamate metabolism**
436 In addition to their role in neuronal energy supply, astrocytes are also vital cell elements in
437 the reuptake and recycling of glutamate in the synapse. Through glutamate transporters
438 (GLAST and GLT-1), astrocytes regulate glutamate release in the synapse by converting
439 glutamate to glutamine through the glutamine synthase (GS) pathway, before releasing it to
440 the extracellular space via glutaminases (GLS1). The released glutamine is subsequently taken
441 up by neurons and re-used as substrate for glutamate production to replenish the presynaptic
442 neurotransmitter pool and help to maintain synaptic transmission (see Figure 5A).
443 We analyzed the mRNA and protein levels of the enzymes involved in the glutamate-
444 glutamine cycling, such as GLAST, GLT-1, GS and GLS1 at several time points after
445 peripheral surgery.

By qRT-PCR we found a profound increase in the mRNA levels of the enzyme gs at 6- and 24h (Figure 5B; **p=0.001; S6H vs. C; n=6-15 animals; **p=0.005; S24H vs. C; n=5-15 animals; one-way ANOVA, Fisher's multiple comparisons test) followed by a drastic reduction at 72h post-surgery (*p=0.04, S72H vs. C; n=5-15 animals; one-way ANOVA, Fisher's multiple comparisons test. Similarly, we found a reduction in protein at 72h post-surgery (Figure 5C and D, *p=0.019, S72H vs. C; n=5 animals/group). Gene expression of gls1 showed a decrease at 24- and 72h after surgery (Figure 5B; *p=0.01, S24H vs. C; *p=0.02, S72H vs. C; 5-15 animals; one-way ANOVA, Fisher's multiple comparisons test), although no changes at the protein level were detected (Figure 5C and D).

6. Functional and structural neuronal synaptic changes occur in the hippocampus at 72h post-surgery

To further explore how tibia fracture affects the glutamatergic system we analyzed the proteins levels of the two most common subunits of the AMPA-Rs (GluA1 and GluA2) by western blot. At 72h, we found a profound increase in the GluA1 compared to controls (Figure 6A (left) and C; **p=0.004; C vs. 72H; n=5-6 animals; one-way ANOVA, Fisher's multiple comparisons test) and a reduction in the GluA2 subunit (Figure 6A (right) and C; *p=0.01; C vs. S72H; n=5-6 animals; one-way ANOVA, Fisher's multiple comparisons test).

In addition, we analyzed the glial glutamate transporters, GLAST and GLT-1, at the same time points (24h and 72h-post-surgery). At 72h, we found a reduction in the protein GLAST (Figure 6B (left) and C; **p=0.0017; C vs. 72H; n=5-6 animals; one-way ANOVA, Fisher's multiple comparisons test) but no changes in GLT-1 (Figure 6B (right) and C; p=0.9; n=5-6 animals one-way ANOVA, Fisher's multiple comparisons test).

In addition to its role in glutamate recycling, GLAST plays an essential role in terminating synaptic transmission and maintaining safety levels of extracellular glutamate, since excessive

amounts of glutamate would cause excitotoxicity via glutamate receptors (Figure 6D). Similarly, alterations in AMPA-Rs subunit composition and reduced GLAST have been associated with increased glutamatergic transmission (Gómez-Galán et al., 2016; 2013). We finally investigated neuronal synaptic transmission after peripheral trauma by whole-cell patch clamp recordings from CA1 pyramidal cells measuring spontaneous excitatory postsynaptic currents (sEPSCs) at 24h and 72h post-surgery. While at 24h, the frequency (Figure 6E (top); Hz: 1.5 ± 0.2 vs. 2± 0.3; C vs. S24H; unpaired t-test; t=1.025, df=24; p=0.3; n=8-18 cells (4-6 animals/group)) and the amplitude (Figure 6E (bottom) pA: 18.5 ± 0.6 vs. 18.5 ± 0.6; C vs. S24H; unpaired t-test; t=0,0013, df=24; p=0.99; n=8-18 cells (4-6 animals/group)) of the sEPSCs events were similar to control animals, at 72h we detected an increase in both the frequency (Figure 6F (top); Hz: 3.2 ± 0.3 vs. 5.5 ± 0.6; C vs. S72H; unpaired t-test; t=3.319, df=35.22; **p=0.002; n=22-26 cells (7 animals/group) and amplitude (Figure 6F (bottom); pA: 17.9 ± 0.7 vs. 21 ± 0.8; C vs. S72H; unpaired t-test; t=2.848, df=46; **p=0.007; n=22-26 cells (7 animals/group)) of sEPSCs compared to control, reflecting an increase in glutamatergic transmission. This increase in excitability may suggest an imbalance between the glutamatergic and the GABAergic (inhibitory) system. To rule out this hypothesis we analyzed spontaneous inhibitory postsynaptic currents (sIPSCs) from CA1 pyramidal cells at 72h. We did not find any difference between control and surgery-treated animals (Figure 6G; Freq: p=0.79; Ampl: p=0.27; t-test; n=9-13 cells (3 animals/group)).

Discussion

The overarching aim of the present study was to determine the underlying temporal alterations associated with systemic immune activation after peripheral surgery on brain neuronal-glial function within hippocampal neuronal circuits of relevance for cognitive processing. Here, we uncover a series of astrocyte and neuronal metabolic, structural and physiological changes in the hippocampus, which reinforce the idea of a dynamic peripheral-to-brain communication and emphasize the role of astrocytes as key intermediaries between peripheral immune events and neuronal processing of information and cognition.

Previous studies have identified a transient disruption of the BBB mediated by the pro-inflammatory milieu after surgery. Through a permeable BBB, cytokines and inflammatory mediators, such as macrophages, were shown to migrate into the hippocampus and modulate its function contributing to postoperative cognitive decline (Terrando et al., 2011; Degos et al., 2013; Yang et al., 2017). These studies also found increased hippocampal mRNA expression of IL-1β and IL-6 at 6h post-surgery, which is in line with the presence of the pro-inflammatory cytokine IL-6 protein in the hippocampus, suggesting that hippocampal inflammation may contribute to the mechanisms responsible for postoperative cognitive changes. Similarly, clinical studies have reported an increase in cytokines levels, including IL-6, in the cerebrospinal fluid of patients after non-neurological surgery (Buvanendran et al., 2006; Bromander et al., 2012; Hirsch et al., 2016).

Astrocytes are critical components of the neurovascular unit, which is a key interface between the periphery and CNS (Kisler et al., 2017). They express cell surface receptors for most cytokines, including IL-1β and IL-6 (Lovatt et al., 2007; Cahoy et al., 2008) and several studies have shown that astrocytes respond to cytokines and inflammatory mediators by altering their morphology and transcriptome profiles, including those related with structural

514 proteins and Ca^{2+} signaling (Hamby et al., 2012; Zamanian et al., 2012; Sofroniew, 2014).
515 Here we detected a decrease gene expression of the astrocyte markers GFAP and AQP4
516 accompanied with profound decrease in GFAP immunoreactivity and alterations in the
517 resting Ca^{2+} signaling at 24h post-surgery. GFAP is an intermediate filament protein
518 involved in the structure and function of the astrocyte's cytoskeleton whose expression is
519 known to be essential for BBB integrity (Liedtke et al., 1996). Similarly, AQP4 is typically co-
520 expressed with GFAP in astrocytes where it is highly polarized to astrocytic end-feet in close
521 contact with blood vessels (Verkman et al., 2006) and participates in BBB formation
522 (Nicchia et al., 2004; Blixt et al., 2015). Although the mechanisms related to BBB integrity
523 after peripheral trauma was not the focus of the study, these new findings together with our
524 previous observation of reduced hippocampal GFAP coverage in astrocytes (Terrando et al.,
525 2013) support previous observation of surgery-induced BBB disruption at 24h post-trauma
526 (Terrando et al., 2011).
527 The reduction in GFAP and AQP4 expression and GFAP coverage observed after surgery
528 may significantly affect astrocytes function, therefore disrupting neuronal circuits involved in
529 higher brain functions, including cognition. Spontaneous or ligand-evoked changes in
530 intracellular Ca^{2+} concentration represent a form of astrocyte excitability that can enable
531 astrocytes to modulate neuronal activity and behavior (Perea et al., 2009; Halassa and
532 Haydon, 2010; Henneberger and Rusakov, 2010). Here, we found reduced astrocytic resting
533 Ca^{2+} signaling evidenced by a reduction in the percentage of active cells within slices and
534 lower Ca^{2+} signal frequency at 24h post-trauma. Opposite to our findings, Ca^{2+} imaging
535 studies from animal models of some brain pathologies, including stroke (Takatsuru et al.,
536 2013), epilepsy (Ding et al., 2007) and AD (Abramov et al., 2003; Kuchibhotla et al., 2009)
537 have shown enhanced astrocytic Ca^{2+} excitability. Although the mechanisms underlying this

increase may differ among these pathologies, a common feature between them, and a difference with our model, is the presence of reactive astrocytes, including up-regulation of GFAP and hypertrophy (Fedele et al., 2005; Osborn et al., 2016; Sims and Yew, 2017). We believe it is possible that some of the aspects related to the mechanisms involved in Ca^{2+} regulation in astrocytes may depend on the origin of the insult or even on the stage of the disorder.

Interesting, studies performed in the hippocampus of a triple transgenic mouse model of AD showed early (at 6 month age) reduction in GFAP surface and volume accompanied by a reduction of the glial branching, which progressed with age. Conversely, astrocytes surrounding amyloid plaques presented the typical reactive characteristics with thick processes and enlarged cell bodies (Olabarria et al., 2010). It would be interesting to apply this model to investigate if such morphological changes also correlate with opposing changes in Ca^{2+} signaling. Notably, functional studies in these animals have shown synaptic plasticity and long-term memory deficits preceding the appearance of amyloid plaques and tangles (Oddo et al., 2003a; Oddo et al., 2003b).

Alterations in intracellular Ca^{2+} signaling after surgery may affect the release of gliotransmitters from astrocytes, including glutamate, ATP, D-serine and GABA with the potential to generate a wide range of functional alterations related to synaptic transmission and plasticity (Parpura et al., 1994; Zonta et al., 2003). In addition, Ca^{2+} evoked release of messengers from astrocytes has also been suggested to regulated the energy supply to the brain (Wang et al., 2009; Bazargani and Attwell, 2016). Here, together with the functional changes observed in astrocytes, we found distinct temporal hippocampal alterations in glucose and glutamate signaling accompanied with changes in whole lactate levels at several time points after peripheral trauma suggesting a neuro-glial metabolic uncoupling in the

562 hippocampus. Lactate is produced by astrocytes via non-oxidative glucose utilization and
563 shuttled to neurons via MCTs where it is used as an energy substrate (Allaman et al., 2011).
564 The early decrease in the gene expression of the two main glucose transporters in the brain
565 (GLUT 1-astrocyte- and GLUT 3-neuron-) accompanied with a reduction in hippocampal
566 lactate levels points to an early alteration in the mechanisms responsible for the uptake of
567 glucose by both, astrocytes and neurons. Interestingly, at 24h post-surgery and coinciding
568 with normal lactate levels, the MCT4, a transporter exclusively located in astrocytes and
569 highly involved in lactate efflux to neurons (Pierre and Pellerin, 2005), shows a transient but
570 profound up-regulation. Supported by the astrocyte-neuron lactate shuttle (ANLS)
571 hypothesis proposed by Pellerini and Magistretti (Pellerin and Magistretti, 1994); but see also
572 (Magistretti, 2009; Barros and Deitmer, 2010), in which lactate release and concomitant
573 glucose uptake in astrocytes is stimulated by sodium-coupled uptake of glutamate from
574 glutamate transporters, we suggest that in our model this temporal up-regulation in astrocytic
575 lactate signaling at 24h post-surgery followed by a decline in lactate levels at 72h may
576 indicate a failed protective attempt from astrocytes to provide with the energy requirements
577 necessary to maintain neuronal activity and the associated brain functions, such as cognition.
578 The functional significance of lactate for cognition after surgery is further supported by
579 other findings showing that interference with lactate transport from astrocytes into neurons
580 impairs synaptic plasticity and memory (Newman et al., 2011; Suzuki et al., 2011).
581 Indeed, parallel to the synaptic plasticity and cognitive dysfunction previously reported
582 (Terrando et al., 2013), at 72h post-surgery we observed the main protein machinery
583 involved in the control of glutamate neurotransmission and energy metabolism (performed
584 by astrocytes) down-regulated, including the glial glutamate (GLAST) and glucose (GLUT-1)
585 transporters, but also the enzymes involved in the glutamate-glutamine cycle, such as GS and

586 GLS1. In addition, the increased neuronal glutamatergic transmission here described at 72h
587 post-surgery in form of increase sEPSCs frequency and amplitude may be the functional
588 consequence of the above mentioned alterations in the reuptake and recycling of glutamate
589 by the astrocyte further accompanied by neuronal alterations in AMPA receptor subunit
590 composition (GluA1 vs. GluA2). Association between decreased GLAST protein levels and
591 increased sEPSCs and impaired synaptic plasticity have also been reported in a rat model of
592 depression characterized with astrocytic morphology alterations and cognitive deficits
593 (Gómez-Galán et al., 2013). Notably, 5 weeks of social isolation in these rats also down-
594 regulated the protein levels of the GluA2 subunit of AMPA receptors (Gómez-Galán et al.,
595 2016). In the hippocampus, the ability of Ca^{2+} to enter the neuronal cell through the AMPA
596 receptor is determined by the GluA1 subunit, which is highly permeable to Ca^{2+} (Cull-Candy
597 et al., 2006). Indeed, it has been shown that activation of GluA2-lacking receptors induces a
598 retrograde signal that enhances release probability at the presynaptic terminal (Lindskog et
599 al., 2010). Other studies have shown increased excitability and impaired synaptic plasticity
600 and memory associated with changes in Ca^{2+}-permeable AMPA receptors (Cull-Candy et al.,
601 2006). Thus, in this surgical model a reduction of GluA2 may increase the probability of
602 glutamate release that together with the reduction in glutamate uptake by the astrocyte, will
603 contribute to increased levels of extracellular glutamate and to a concomitant increase in
604 glutamate transmission. Since astrocytes do also express AMPA receptors further studies are
605 necessary to address if peripheral surgery affect differently glial and neuronal AMPA-R
606 subunit composition and function.
607 In summary, we demonstrate that peripheral surgery following systemic immune activation
608 orchestrates temporal metabolic adaptations in the hippocampus, including alteration in
609 glucose and glutamate signaling in astrocytes, and reduction in brain lactate availability. As a

consequence, the neuro-glial metabolic coupling is compromised as well as the astrocyte and neuronal function suggesting that the decrease in lactate availability in the hippocampus after peripheral trauma might be related to the cognitive impairment observed acutely after trauma.

614 **References**

615 Abramov AY, Canevari L, Duchen MR (2003) Changes in intracellular calcium and
616 glutathione in astrocytes as the primary mechanism of amyloid neurotoxicity. J
617 Neurosci 23:5088-5095.

618 Allaman I, Belanger M, Magistretti PJ (2011) Astrocyte-neuron metabolic relationships: for
619 better and for worse. Trends Neurosci 34:76-87.

620 Banks WA (2005) Blood-brain barrier transport of cytokines: a mechanism for
621 neuropathology. Curr Pharm Des 11:973-984.

622 Banks WA, Kastin AJ, Gutierrez EG (1994) Penetration of interleukin-6 across the murine
623 blood-brain barrier. Neurosci Lett 179:53-56.

624 Banks WA, Kastin AJ, Broadwell RD (1995) Passage of cytokines across the blood-brain
625 barrier. Neuroimmunomodulation 2:241-248.

626 Barros LF, Deitmer JW (2010) Glucose and lactate supply to the synapse. Brain Res Rev
627 63:149-159.

628 Bazargani N, Attwell D (2016) Astrocyte calcium signaling: the third wave. Nat Neurosci
629 19:182-189.

630 Beloosesky Y, Hendel D, Weiss A, Hershkovitz A, Grinblat J, Pirotsky A, Barak V (2007)
631 Cytokines and C-reactive protein production in hip-fracture-operated elderly
632 patients. J Gerontol A Biol Sci Med Sci 62:420-426.

633 Birch AM, Katsouri L, Sastre M (2014) Modulation of inflammation in transgenic models of
634 Alzheimer's disease. J Neuroinflammation 11:25.

635 Blixt J, Svensson M, Gunnarson E, Wanecek M (2015) Aquaporins and blood-brain barrier
636 permeability in early edema development after traumatic brain injury. Brain Res
637 1611:18-28.

638 Bromander S, Anckarsater R, Kristiansson M, Blennow K, Zetterberg H, Anckarsater H,
639 Wass CE (2012) Changes in serum and cerebrospinal fluid cytokines in response to
640 non-neurological surgery: an observational study. J Neuroinflammation 9:242.
641 Buvanendran A, Kroin JS, Berger RA, Hallab NJ, Saha C, Negrescu C, Moric M, Caicedo
642 MS, Tuman KJ (2006) Upregulation of prostaglandin E2 and interleukins in the
643 central nervous system and peripheral tissue during and after surgery in humans.
644 Anesthesiology 104:403-410.
645 Cahoy JD, Emery B, Kaushal A, Foo LC, Zamanian JL, Christopherson KS, Xing Y,
646 Lubischer JL, Krieg PA, Krupenko SA, Thompson WJ, Barres BA (2008) A
647 transcriptome database for astrocytes, neurons, and oligodendrocytes: a new
648 resource for understanding brain development and function. J Neurosci 28:264-278.
649 Cibelli M, Fidalgo AR, Terrando N, Ma D, Monaco C, Feldmann M, Takata M, Lever IJ,
650 Nanchahal J, Fanselow MS, Maze M (2010) Role of interleukin-1beta in
651 postoperative cognitive dysfunction. Ann Neurol 68:360-368.
652 Collins LM, Toulouse A, Connor TJ, Nolan YM (2012) Contributions of central and
653 systemic inflammation to the pathophysiology of Parkinson's disease.
654 Neuropharmacology 62:2154-2168.
655 Cull-Candy S, Kelly L, Farrant M (2006) Regulation of Ca2+-permeable AMPA receptors:
656 synaptic plasticity and beyond. Curr Opin Neurobiol 16:288-297.
657 Degos V, Vacas S, Han Z, van Rooijen N, Gressens P, Su H, Young WL, Maze M (2013)
658 Depletion of bone marrow-derived macrophages perturbs the innate immune
659 response to surgery and reduces postoperative memory dysfunction. Anesthesiology
660 118:527-536.

661 Ding S, Fellin T, Zhu Y, Lee SY, Auberson YP, Meaney DF, Coulter DA, Carmignoto G,
662 Haydon PG (2007) Enhanced astrocytic Ca2+ signals contribute to neuronal
663 excitotoxicity after status epilepticus. J Neurosci 27:10674-10684.
664 Fedele DE, Gouder N, Guttinger M, Gabernet L, Scheurer L, Rulicke T, Crestani F, Boison
665 D (2005) Astrogliosis in epilepsy leads to overexpression of adenosine kinase,
666 resulting in seizure aggravation. Brain 128:2383-2395.
667 Fidalgo AR, Cibelli M, White JP, Nagy I, Maze M, Ma D (2011) Systemic inflammation
668 enhances surgery-induced cognitive dysfunction in mice. Neuroscience letters
669 498:63-66.
670 Forsberg A, Cervenka S, Jonsson Fagerlund M, Rasmussen LS, Zetterberg H, Erlandsson
671 Harris H, Stridh P, Christensson E, Granstrom A, Schening A, Dymmel K, Knave
672 N, Terrando N, Maze M, Borg J, Varrone A, Halldin C, Blennow K, Farde L,
673 Eriksson LI (2017) The immune response of the human brain to abdominal surgery.
674 Ann Neurol 81:572-582.
675 Hill RA, Grutzendler J (2014) In vivo imaging of oligodendrocytes with sulforhodamine 101.
676 Nature methods 11:1081-1082.
677 Gomez-Galan M, De Bundel D, Van Eeckhaut A, Smolders I, Lindskog M (2013)
678 Dysfunctional astrocytic regulation of glutamate transmission in a rat model of
679 depression. Mol Psychiatry 18:582-594.
680 Gomez-Galan M, Femenia T, Aberg E, Graae L, Van Eeckhaut A, Smolders I, Brene S,
681 Lindskog M (2016) Running Opposes the Effects of Social Isolation on Synaptic
682 Plasticity and Transmission in a Rat Model of Depression. PLoS One 11:e0165071.
683 Gutierrez EG, Banks WA, Kastin AJ (1994) Blood-borne interleukin-1 receptor antagonist
684 crosses the blood-brain barrier. J Neuroimmunol 55:153-160.

685 Halassa MM, Haydon PG (2010) Integrated brain circuits: astrocytic networks modulate
686 neuronal activity and behavior. Annu Rev Physiol 72:335-355.
687 Hamby ME, Coppola G, Ao Y, Geschwind DH, Khakh BS, Sofroniew MV (2012)
688 Inflammatory mediators alter the astrocyte transcriptome and calcium signaling
689 elicited by multiple G-protein-coupled receptors. J Neurosci 32:14489-14510.
690 Henneberger C, Rusakov DA (2010) Synaptic plasticity and Ca2+ signalling in astrocytes.
691 Neuron Glia Biol 6:141-146.
692 Hirsch J, Vacas S, Terrando N, Yuan M, Sands LP, Kramer J, Bozic K, Maze MM, Leung
693 JM (2016) Perioperative cerebrospinal fluid and plasma inflammatory markers after
694 orthopedic surgery. J Neuroinflammation 13:211.
695 Kafitz KW, Meier SD, Stephan J, Rose CR (2008) Developmental profile and properties of
696 sulforhodamine 101--Labeled glial cells in acute brain slices of rat hippocampus. J
697 Neurosci Methods 169:84-92.
698 Kisler K, Nelson AR, Montagne A, Zlokovic BV (2017) Cerebral blood flow regulation and
699 neurovascular dysfunction in Alzheimer disease. Nature reviews Neuroscience
700 18:419-434.
701 Kline R, Wong E, Haile M, Didehvar S, Farber S, Sacks A, Pirraglia E, de Leon MJ, Bekker
702 A (2016) Peri-Operative Inflammatory Cytokines in Plasma of the Elderly Correlate
703 in Prospective Study with Postoperative Changes in Cognitive Test Scores. Int J
704 Anesthesiol Res 4:313-321.
705 Kuchibhotla KV, Lattarulo CR, Hyman BT, Bacskai BJ (2009) Synchronous hyperactivity
706 and intercellular calcium waves in astrocytes in Alzheimer mice. Science 323:1211-
707 1215.

708 Lebson L, Nash K, Kamath S, Herber D, Carty N, Lee DC, Li Q, Szekeres K, Jinwal U,
709 Koren J, Dickey CA, Gottschall PE, Morgan D, Gordon MN (2010) Trafficking
710 CD11b-positive blood cells deliver therapeutic genes to the brain of amyloid-
711 depositing transgenic mice. J Neurosci 30:9651-9658.
712 Liedtke W, Edelmann W, Bieri PL, Chiu FC, Cowan NJ, Kucherlapati R, Raine CS (1996)
713 GFAP is necessary for the integrity of CNS white matter architecture and long-term
714 maintenance of myelination. Neuron 17:607-615.
715 Lindskog M, Li L, Groth RD, Poburko D, Thiagarajan TC, Han X, Tsien RW (2010)
716 Postsynaptic GluA1 enables acute retrograde enhancement of presynaptic function
717 to coordinate adaptation to synaptic inactivity. Proc Natl Acad Sci U S A 107:21806-
718 21811.
719 Lovatt D, Sonnewald U, Waagepetersen HS, Schousboe A, He W, Lin JH, Han X, Takano
720 T, Wang S, Sim FJ, Goldman SA, Nedergaard M (2007) The transcriptome and
721 metabolic gene signature of protoplasmic astrocytes in the adult murine cortex. J
722 Neurosci 27:12255-12266.
723 Lu SM, Yu CJ, Liu YH, Dong HQ, Zhang X, Zhang SS, Hu LQ, Zhang F, Qian YN, Gui B
724 (2015) S100A8 contributes to postoperative cognitive dysfunction in mice
725 undergoing tibial fracture surgery by activating the TLR4/MyD88 pathway. Brain,
726 behavior, and immunity 44:221-234.
727 Magistretti PJ (2009) Role of glutamate in neuron-glia metabolic coupling. Am J Clin Nutr
728 90:875S-880S.
729 Newman LA, Korol DL, Gold PE (2011) Lactate produced by glycogenolysis in astrocytes
730 regulates memory processing. PloS one 6:e28427.

731 Nicchia GP, Nico B, Camassa LM, Mola MG, Loh N, Dermietzel R, Spray DC, Svelto M,
732 Frigeri A (2004) The role of aquaporin-4 in the blood-brain barrier development and
733 integrity: studies in animal and cell culture models. Neuroscience 129:935-945.
734 Oddo S, Caccamo A, Kitazawa M, Tseng BP, LaFerla FM (2003a) Amyloid deposition
735 precedes tangle formation in a triple transgenic model of Alzheimer's disease.
736 Neurobiol Aging 24:1063-1070.
737 Oddo S, Caccamo A, Shepherd JD, Murphy MP, Golde TE, Kayed R, Metherate R, Mattson
738 MP, Akbari Y, LaFerla FM (2003b) Triple-transgenic model of Alzheimer's disease
739 with plaques and tangles: intracellular Abeta and synaptic dysfunction. Neuron
740 39:409-421.
741 Olabarria M, Noristani HN, Verkhratsky A, Rodriguez JJ (2010) Concomitant astroglial
742 atrophy and astrogliosis in a triple transgenic animal model of Alzheimer's disease.
743 Glia 58:831-838.
744 Osborn LM, Kamphuis W, Wadman WJ, Hol EM (2016) Astrogliosis: An integral player in
745 the pathogenesis of Alzheimer's disease. Prog Neurobiol 144:121-141.
746 Parpura V, Basarsky TA, Liu F, Jeftinija K, Jeftinija S, Haydon PG (1994) Glutamate-
747 mediated astrocyte-neuron signalling. Nature 369:744-747.
748 Pellerin L, Magistretti PJ (1994) Glutamate uptake into astrocytes stimulates aerobic
749 glycolysis: a mechanism coupling neuronal activity to glucose utilization. Proc Natl
750 Acad Sci U S A 91:10625-10629.
751 Perea G, Navarrete M, Araque A (2009) Tripartite synapses: astrocytes process and control
752 synaptic information. Trends Neurosci 32:421-431.
753 Perry VH, Holmes C (2014) Microglial priming in neurodegenerative disease. Nature reviews
754 Neurology 10:217-224.

755 Perry VH, Newman TA, Cunningham C (2003) The impact of systemic infection on the
756 progression of neurodegenerative disease. Nat Rev Neurosci 4:103-112.
757 Perry VH, Cunningham C, Holmes C (2007) Systemic infections and inflammation affect
758 chronic neurodegeneration. Nature reviews Immunology 7:161-167.
759 Pierre K, Pellerin L (2005) Monocarboxylate transporters in the central nervous system:
760 distribution, regulation and function. J Neurochem 94:1-14.
761 Romero-Calvo I, Ocon B, Martinez-Moya P, Suarez MD, Zarzuelo A, Martinez-Augustin O,
762 de Medina FS (2010) Reversible Ponceau staining as a loading control alternative to
763 actin in Western blots. Anal Biochem 401:318-320.
764 Rosczyk HA, Sparkman NL, Johnson RW (2008) Neuroinflammation and cognitive function
765 in aged mice following minor surgery. Experimental gerontology 43:840-846.
766 Saederup N, Cardona AE, Croft K, Mizutani M, Cotleur AC, Tsou CL, Ransohoff RM,
767 Charo IF (2010) Selective chemokine receptor usage by central nervous system
768 myeloid cells in CCR2-red fluorescent protein knock-in mice. PLoS One 5:e13693.
769 Schindelin J, Arganda-Carreras I, Frise E, Kaynig V, Longair M, Pietzsch T, Preibisch S,
770 Rueden C, Saalfeld S, Schmid B, Tinevez JY, White DJ, Hartenstein V, Eliceiri K,
771 Tomancak P, Cardona A (2012) Fiji: an open-source platform for biological-image
772 analysis. Nat Methods 9:676-682.
773 Sims NR, Yew WP (2017) Reactive astrogliosis in stroke: Contributions of astrocytes to
774 recovery of neurological function. Neurochem Int 107:88-103.
775 Sofroniew MV (2014) Multiple roles for astrocytes as effectors of cytokines and
776 inflammatory mediators. Neuroscientist 20:160-172.

777 Suzuki A, Stern SA, Bozdagi O, Huntley GW, Walker RH, Magistretti PJ, Alberini CM
778 (2011) Astrocyte-neuron lactate transport is required for long-term memory
779 formation. Cell 144:810-823.
780 Takatsuru Y, Eto K, Kaneko R, Masuda H, Shimokawa N, Koibuchi N, Nabekura J (2013)
781 Critical role of the astrocyte for functional remodeling in contralateral hemisphere of
782 somatosensory cortex after stroke. J Neurosci 33:4683-4692.
783 Terrando N, Monaco C, Ma D, Foxwell BM, Feldmann M, Maze M (2010) Tumor necrosis
784 factor-alpha triggers a cytokine cascade yielding postoperative cognitive decline. Proc
785 Natl Acad Sci U S A 107:20518-20522.
786 Terrando N, Gomez-Galan M, Yang T, Carlstrom M, Gustavsson D, Harding RE, Lindskog
787 M, Eriksson LI (2013) Aspirin-triggered resolvin D1 prevents surgery-induced
788 cognitive decline. FASEB J 27:3564-3571.
789 Terrando N, Eriksson LI, Ryu JK, Yang T, Monaco C, Feldmann M, Jonsson Fagerlund M,
790 Charo IF, Akassoglou K, Maze M (2011) Resolving postoperative
791 neuroinflammation and cognitive decline. Ann Neurol 70:986-995.
792 Thevenaz P, Ruttimann UE, Unser M (1998) A pyramid approach to subpixel registration
793 based on intensity. IEEE Trans Image Process 7:27-41.
794 Verkman AS, Binder DK, Bloch O, Auguste K, Papadopoulos MC (2006) Three distinct
795 roles of aquaporin-4 in brain function revealed by knockout mice. Biochim Biophys
796 Acta 1758:1085-1093.
797 Wang X, Takano T, Nedergaard M (2009) Astrocytic calcium signaling: mechanism and
798 implications for functional brain imaging. Methods in molecular biology (Clifton, NJ)
799 489:93-109.

800 Yang S, Gu C, Mandeville ET, Dong Y, Esposito E, Zhang Y, Yang G, Shen Y, Fu X, Lo
801 EH, Xie Z (2017) Anesthesia and Surgery Impair Blood-Brain Barrier and Cognitive
802 Function in Mice. Frontiers in immunology 8:902.
803 Zamanian JL, Xu L, Foo LC, Nouri N, Zhou L, Giffard RG, Barres BA (2012) Genomic
804 analysis of reactive astrogliosis. J Neurosci 32:6391-6410.
805 Zonta M, Sebelin A, Gobbo S, Fellin T, Pozzan T, Carmignoto G (2003) Glutamate-
806 mediated cytosolic calcium oscillations regulate a pulsatile prostaglandin release from
807 cultured rat astrocytes. J Physiol 553:407-414.
808
809

Figure legends

Figure 1. Brain cytokine levels after peripheral surgery

Hippocampal cytokine expression was assessed at 6- and 72h post-surgery using a multiplex assay for 10 different cytokines. While the pro-inflammatory cytokine IL-6 is increased at 6h after surgery (IL6: ***p=0.0002 C vs. S6H, #p=0.01 S6H vs. S72H, One-way ANOVA, Fisher's multiple comparison test) IL-β is decreased (*p=0.03 C vs. S6H; ##p=0.0095 S6H vs. S72H). Empty dots on each graph represent individuals. Initially, numbers of animals were similar for each cytokine (C: n=10; S6H: n=5; S72H: n=5). However, those values which lay bellow the detectable range were excluded from the analysis. N.D: non-detectable. All data are presented as the mean ± SEM.

Figure 2. Peripheral surgery regulates expression of astrocytic markers

Analysis of gene expression by qRT PCR of glial cells markers at 6-24- and 72h post-surgery. The astrocytic markers **A.** glial fibrillary acidic protein (GFAP) and **B.** Aquaporin 4 (AQP4) are down-regulated at 24- and 72h post-surgery. (gfap: *p=0.02 C vs. S24H and *p=0.04 C vs. S72H; n=5-16 animals; Aqp4: *p=0.04 at C vs. S24H and *p=0.01 C vs. S72h; n=4-12 One-way ANOVA, Fisher's multiple comparison test). All data are presented as the mean ± SEM.

Figure 3. Resting calcium signaling is decreased in the hippocampal astrocytic network after surgery

A. Representative hippocampal slice from a control animal loaded with the astrocytic marker S101 (red) and the calcium dye OGB-1M (green) and the corresponding overlay (yellow). **B.** A frame of a time-lapse imaging from the same slice in **A** with the active cells highlighted by

a yellow circle. **C.** Traces of calcium spontaneous activity of the astrocytes outlined in **C** (from a control animal; **left**) and from a surgery-treated animal 24h-post surgery (S24H; **right**). **D.** 24h after surgery there is a decrease in the number of S101+ cells (**p=0.002; unpaired t-test; n=19-14 slices). **E-F-G.** Hippocampal GFAP immunohistochemistry shows similar number of $GFAP^+$ cells between control and surgery-treated animals (n=8-10 animals) (**E**) but profound decrease in GFAP immunoreactivity after surgery (**F-G;** **p=0.0019; unpaired t-test; n=6-9 animals). **H.** The distribution of the percentage of active astrocytes is reduced after surgery (###p=0.0001, unpaired t-test Welch's correction; F test to compare variances; F: 10.36; DFn: 18; Dfd: 13; n=14-19 slices). **I.** At 24h-post surgery the frequency of the spontaneous (*p=0.01; unpaired t-test with Welch´s correction; n=19-14 slices (4-5 animals/group)) and **J.** ATP-evoked calcium spikes is decreased (*p=0.05; unpaired t-test with Welch´s correction; n=10-15 slices (7 animals/group). All data are presented as the mean ± SEM.

Figure 4. Glucose and lactate transporters deficiency is accompanied with changes in hippocampal lactate levels after peripheral surgery

A. Schematic diagram of the astrocyte–neuron lactate shuttle. **B.** Lactate levels in the whole hippocampal homogenates are decreased at 6- and 72h post-surgery (*p=0.01, C vs. S6H and *p=0.047, C vs. S72H; One-way ANOVA, Fisher's multiple comparison test; n= 5 mice/ group). **C.** Astrocyte glucose transporter GLUT1 and neuronal GLUT3 mRNA expression is decreased at 6h-post-surgery (Glut-1: **p=0.031; glut-3: ***p<0.0022; One-way ANOVA, Fisher's multiple comparison test; n= 5-15 mice/group). Protein levels were decreased at 72h after surgery for GLUT-1 *p=0.019, S72H vs. C; n=5 mice/group) and decreased at 24h and 72h for GLUT-3 **p=0.001, S24H vs. C; **p=0.002, S72H vs. C; n= 5

mice/group). **D.** Monocarboxilate transporters mRNA expression is also affected after surgery (Mct1: *p=0.05 C vs. S6H, *P=0.032 C vs. S72H; mct2: p=0.054 C vs. 6H; *p=0.042 C vs. S72H; mct4: ****p<0.0001 C vs. S72H; One-way ANOVA, Fisher's multiple comparison test; n=5-15 mice/group). E. Corresponding protein blots for each protein (normalized to Ponceau S). Triplicates in each group represent different animals. All data are presented as the mean ± SEM.

Figure 5. Peripheral surgery affects hippocampal enzymes involved in glutamate metabolism

A. Schematic illustration outlining the glutamate-glutamine cycle between astrocyte and neurons. **B.** Astrocyte glutamine synthase (GS) and Neuronal Glutaminase-1 (GLS1) mRNA expression and **C.** protein levels (*p<0.05, **p<0.01 vs. C, One-way ANOVA, Fisher's multiple comparison test; mRNA: n= 5-15 mice/group; protein: n= 5 mice/group). **D**. Panels represent the corresponding protein blots for each protein (normalized to Ponceau S). Triplicates in each group represent different animals. All data are presented as the mean ± SEM.

Figure 6. Functional and structural neuronal synaptic changes occur in the hippocampus at 72h post-surgery

A. AMPA receptor subunits GluA1 and GluA2 are affected at 72h post-surgery (**left**, GLUA1: **p=0.0017 C vs. S72H; **right**, GLUA2: *p=0.01 C vs. S72H; One-way ANOVA, Fisher's multiple comparison test; n= 3-6 animals/group). **B.** GLAST is down-regulated at 72h post-surgery (**left**, GLAST: **p=0.0017 c vs. S72H, One-way ANOVA, Fisher's multiple comparison test; n= 3-6 animals/group) but not effect is observed in GLT-1

(**right**). **C.** Representative blots of individual hippocampal samples from control, 24- and 72h surgery-treated mice of the two most common subunits of the AMPARs (GLUR1 and GLUR2) and the astrocytic glutamate transporters (GLAST and GLT-1) (normalized to the transfer Ponceau S). D. Schematic illustration outlining the neuronal glutamate synapse (left) and the representative examples of whole-cell patch clamp recordings from a CA1 pyramidal cell from control (**top-right**) and surgery-treated mouse 72h post-surgery (**bottom-right**). **E**. At 24h the frequency (**top**) and amplitude (**bottom**) remains normal (n= 8-18 cells; 4-6 animals/group). **F.** At 72h post-surgery the frequency (**top**) and amplitude (**bottom**) of sEPSCs is increased in the CA1 area of surgery-treated mice (**p=0.002, t-test; n=22-26 cells; 7-11 animals/group). **G.** The inhibitory (GABA) system remains unaffected at 72h post-surgery (n= 9-13 cells; 3 animals/group). All data are presented as the mean ± SEM.

Figure 7. Schematic illustration summarizing the effect of orthopedic mice surgery on hippocampal astrocyte-neuron metabolism, structure and function

Orthopedic surgery in mice (i.e. tibia fracture) temporally orchestrates a series of hippocampal metabolic, structural and functional changes first in the astrocyte and later in neurons that emphasize the role of astrocytes as key intermediaries between peripheral immune events and neuronal processing information and potentially to cognition. Red arrows depict decreased mRNA/protein levels.

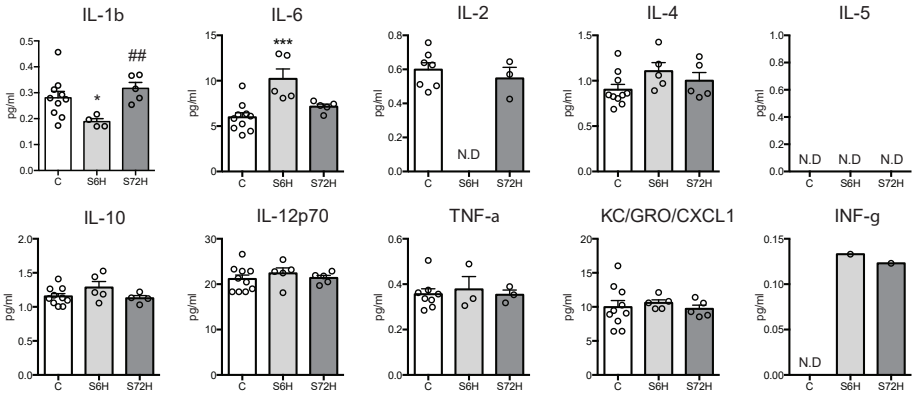

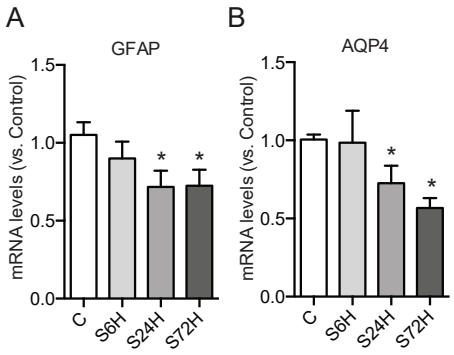

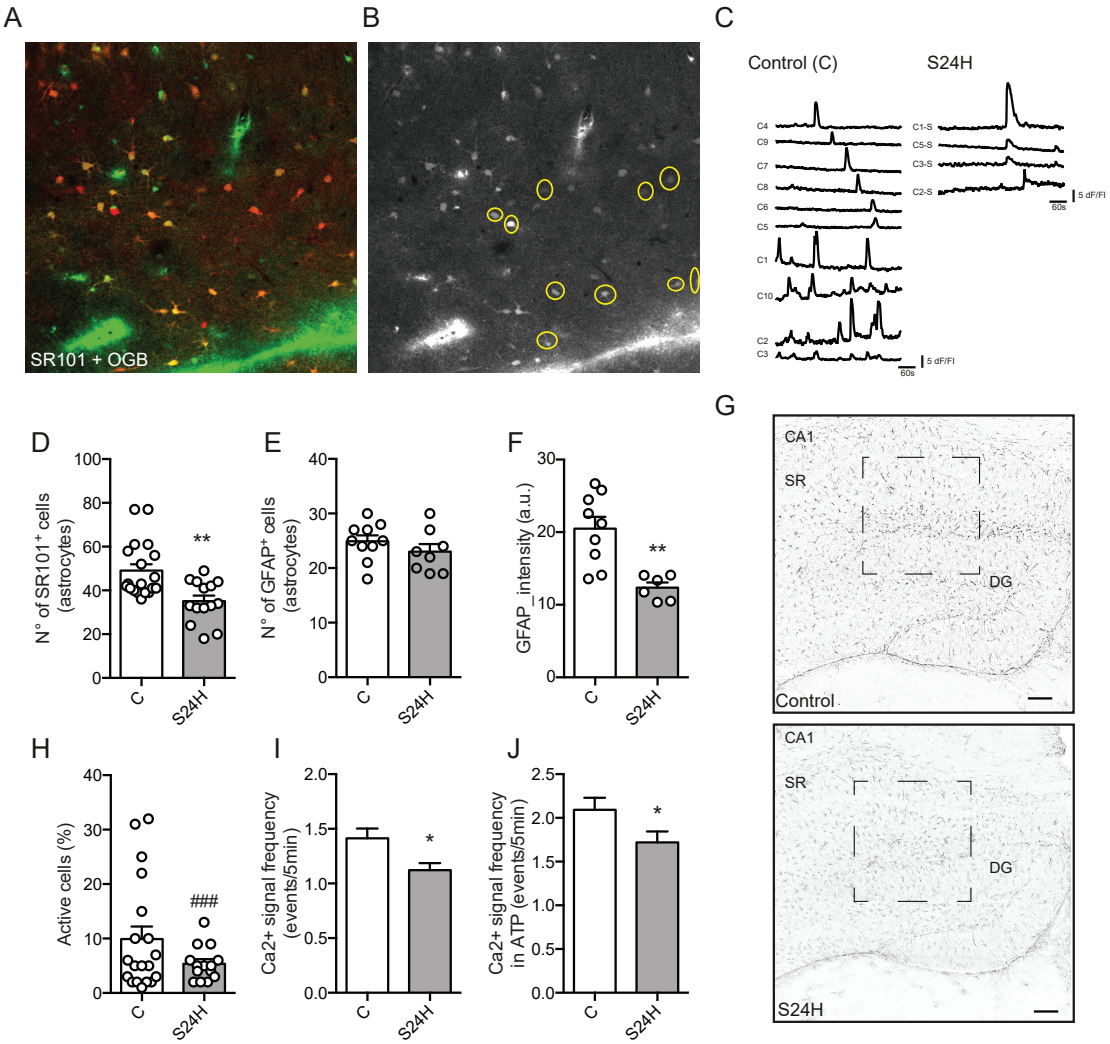

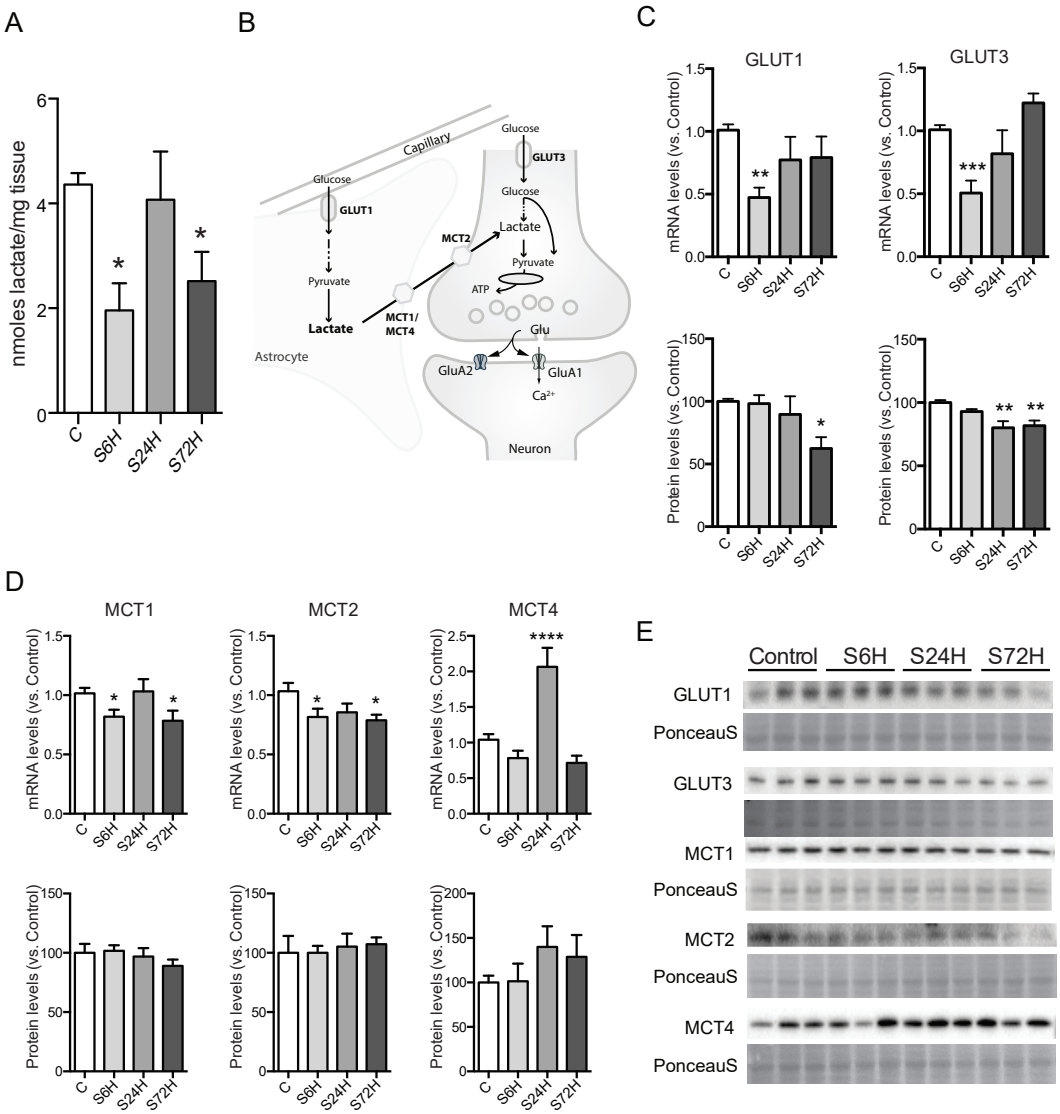

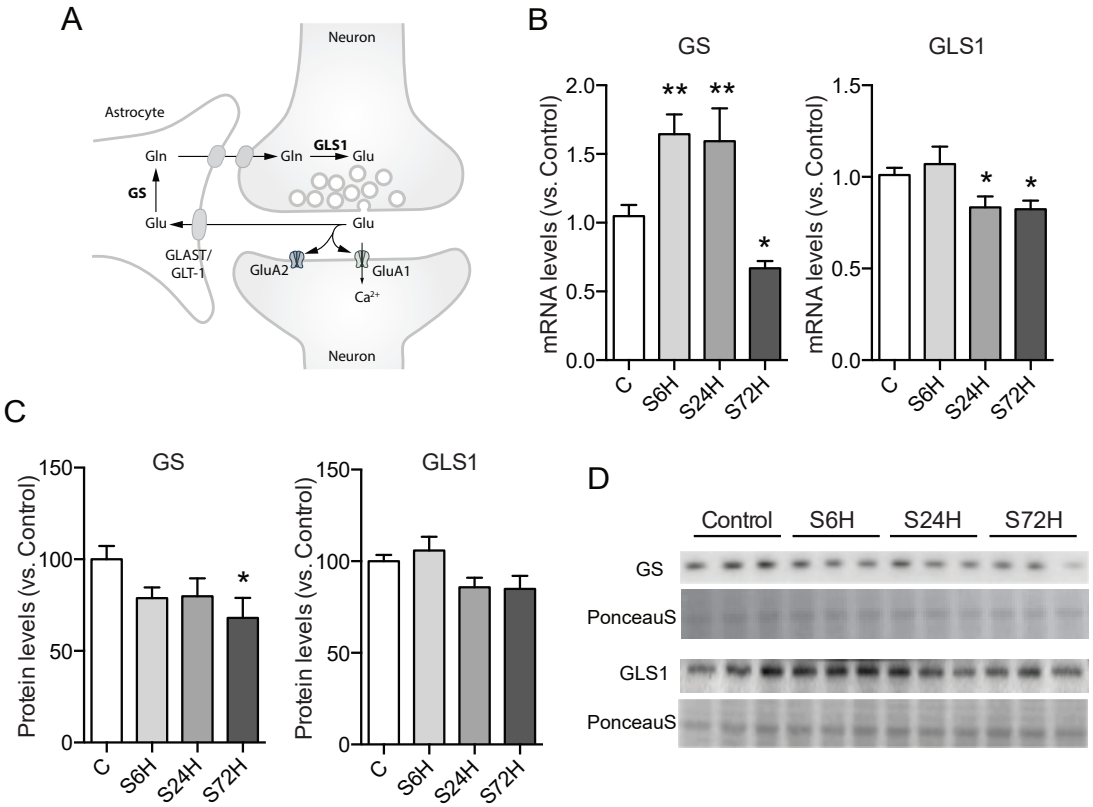

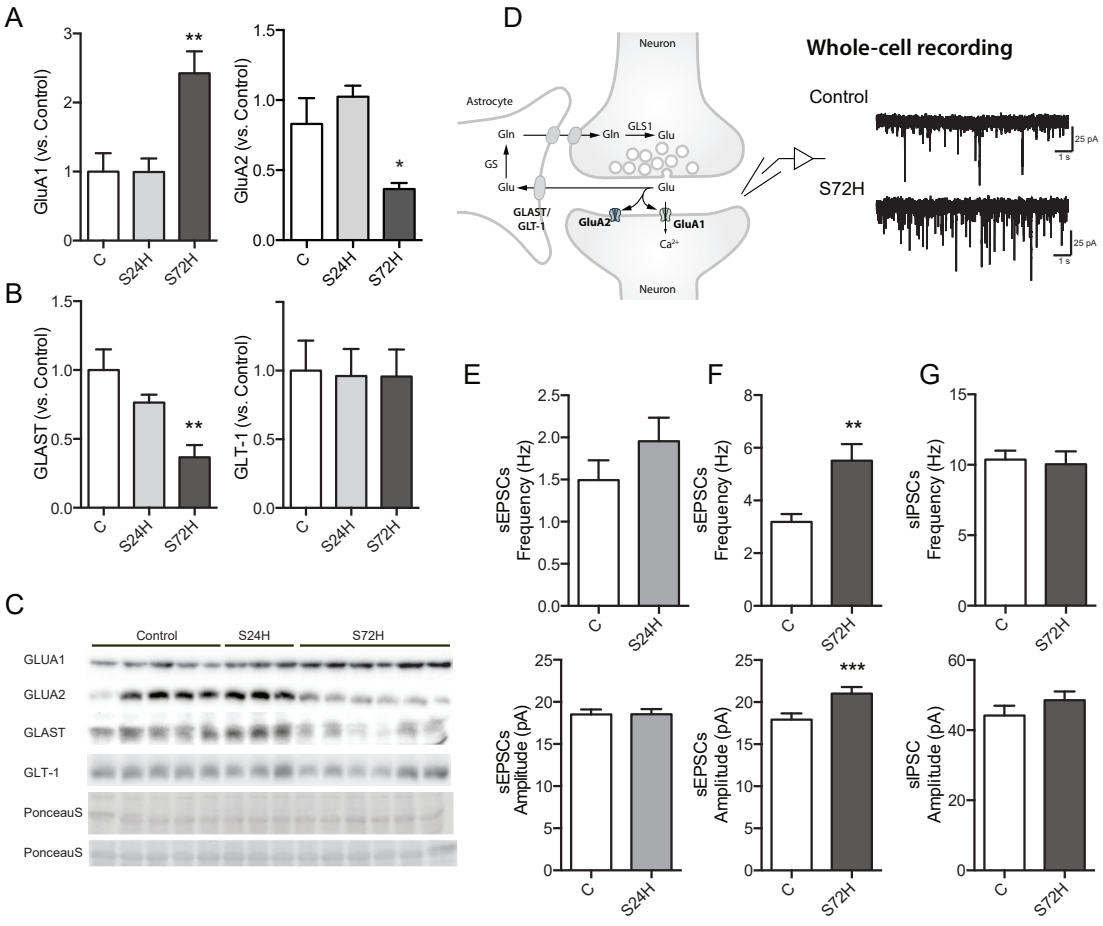

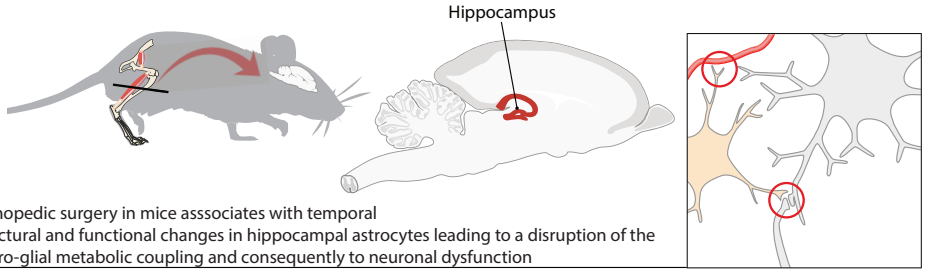

Orthopedic surgery in mice asssociates with temporal structural and functional changes in hippocampal astrocytes leading to a disruption of the neuro-glial metabolic coupling and consequently to neuronal dysfunction